

Genetic and biochemical characterization of a radical SAM enzyme required for post-translational glutamine methylation of methyl-coenzyme M reductase

Roy J. Rodriguez Carrero,¹ Cody T. Lloyd,² Janhavi Borkar,³ Shounak Nath,⁴ Liviu M. Mirica,⁴ Satish Nair,^{3,5} Squire J. Booker,^{2,6,7} William Metcalf¹

AUTHOR AFFILIATIONS See affiliation list on p. 12.

ABSTRACT Methyl-coenzyme M reductase (MCR), the key catalyst in the anoxic production and consumption of methane, contains an unusual 2-methylglutamine residue within its active site. *In vitro* data show that a B12-dependent radical SAM (rSAM) enzyme, designated MgmA, is responsible for this post-translational modification (PTM). Here, we show that two different MgmA homologs are able to methylate MCR *in vivo* when expressed in *Methanosarcina acetivorans*, an organism that does not normally possess this PTM. *M. acetivorans* strains expressing MgmA showed small, but significant, reductions in growth rates and yields on methylophilic substrates. Structural characterization of the Ni(II) form of Gln-methylated *M. acetivorans* MCR revealed no significant differences in the protein fold between the modified and unmodified enzyme; however, the purified enzyme contained the heterodisulfide reaction product, as opposed to the free cofactors found in eight prior *M. acetivorans* MCR structures, suggesting that substrate/product binding is altered in the modified enzyme. Structural characterization of MgmA revealed a fold similar to other B12-dependent rSAMs, with a wide active site cleft capable of binding an McrA peptide in an extended, linear conformation.

IMPORTANCE Methane plays a key role in the global carbon cycle and is an important driver of climate change. Because MCR is responsible for nearly all biological methane production and most anoxic methane consumption, it plays a major role in setting the atmospheric levels of this important greenhouse gas. Thus, a detailed understanding of this enzyme is critical for the development of methane mitigation strategies.

KEYWORDS methyl-coenzyme M reductase, methanogenesis, post-translational modification, archaea, *Methanosarcina*

Methyl-coenzyme M reductase (MCR) is the central catalyst in the biological methane cycle and plays a key role in climate homeostasis due the potent greenhouse potential of this gas. The enzyme is found solely in methanogenic and methanotrophic archaea, which are ubiquitous microorganisms inhabiting a variety of anoxic environments (1, 2). During methanogenesis, MCR catalyzes the final step of methane production, while it operates in the reverse direction in anoxic methanotrophs, activating methane for subsequent catabolism. Significantly, these reactions comprise key steps of the global carbon cycle, with methanogens producing gigatons of methane annually and anoxic methanotrophs consuming more than 90% of the methane produced in marine sediments (2).

MCR is a highly unusual enzyme, catalyzing the reversible conversion of methyl-coenzyme M (2-methylthioethanesulfonate, methyl-CoM) and coenzyme B (N-7 mercaptoheptanoylthreoninephosphate, CoB) to methane and the heterodisulfide of CoB and

Editor Derek R. Lovley, University of Massachusetts Amherst, Amherst, Massachusetts, USA

Address correspondence to William Metcalf, metcalf@illinois.edu.

The authors declare no conflict of interest.

See the funding table on p. 13.

Received 19 November 2024

Accepted 26 November 2024

Published 8 January 2025

Copyright © 2025 Rodriguez Carrero et al. This is an open-access article distributed under the terms of the [Creative Commons Attribution 4.0 International license](https://creativecommons.org/licenses/by/4.0/).

CoM (CoM-S-S-CoB). Although the mechanism of this reaction has yet to be fully elucidated, current evidence suggests that heterolytic cleavage of methyl-CoM forms a rare methyl radical intermediate that reacts with coenzyme B to produce methane and a CoB radical that recombines with CoM to form CoM-S-S-CoB (3). This intriguing reaction involves a nickel-containing porphyrinoid cofactor, known as F₄₃₀, found solely in MCR and the closely related alkyl-CoM reductases (4). For MCR to be catalytically active, the nickel within F₄₃₀ must be in the Ni(I) oxidation state; however, the cofactor is readily oxidized to an inactive Ni(II) state, which has made *in vitro* biochemical characterization of the enzyme extremely challenging (2).

Structural characterization of MCR from *Methanothermobacter marburgensis* showed the enzyme to be an intertwined hexamer with two copies each of three subunits ($\alpha_2/\beta_2/\gamma_2$), and five post-translationally modified amino acids near the active site on the α subunit: 1-N-methylhistidine, 5-methylarginine, S-methylcysteine, 2-methylglutamine, and thioglycine (5). Characterization of additional MCRs revealed several more post-translationally modified residues, including didehydroaspartate, 6-hydroxytryptophan, 7-hydroxytryptophan, methylisoleucine, and 2-N-methylhistidine (6–11). The distribution of these post-translational modifications (PTMs) varies between species, with some being widely conserved and others being seen only rarely (12). Despite these variations, all characterized MCRs possess at least three post-translationally modified amino acids near the active site, suggesting that the PTMs play an important role in either catalysis or protein stability (2, 12, 13). Although experimental evidence regarding the function of these PTMs is scarce, considerable progress has been made in identifying the genes and enzymes required for these modifications.

The enzyme that converts glycine to thioglycine was identified as a homolog of ones that catalyze similar sulfur chemistry during synthesis of thiazole natural products (14). The encoding gene, designated *ycaO*, is often found adjacent to the MCR operon, providing further support for this proposal. *Methanosarcina acetivorans* mutants with deletions of *ycaO* produce MCR without thioglycine, establishing its role in synthesis of this PTM (14). In addition, three different YcaO homologs have been shown to convert glycine to thioglycine *in vitro* (15).

Two types of enzymes are involved in post-translational methylations of MCR. Simple nucleophilic substitutions by canonical SAM-dependent methyltransferases are routinely used for N and S methylations, like those found in S-methylcysteine and N-methylhistidine. Consistent with this idea, the canonical SAM-dependent methyltransferase encoded by the *mcmA* gene is responsible for the S-methylcysteine modification, based on absence of this PTM in *M. acetivorans mcmA* deletion mutants (16). In contrast, methylation at the C2 position of glutamine, or the C5 position of arginine, requires stronger chemistry, such as that used by radical SAM (rSAM) enzymes (17). In particular, the B12-dependent subfamily of rSAMs commonly catalyze transfer of methyl groups to *sp*³-hybridized carbon atoms like those in 2-methylglutamine and 5-methylarginine PTMs (18). The *mamA* gene (also known *mmp10* or *mmpX*) encodes a member of this family that is responsible for 5-methylarginine synthesis as shown by the failure of *M. acetivorans*, and *Methanococcus maripaludis mamA* mutants make this PTM, and the ability of purified MamA is able to methylate peptide substrate mimics (16, 19, 20). The structure, substrate specificity and redox characteristics of *M. acetivorans* MamA have recently been determined, providing the clearest picture to date of the enzymatic mechanism for members of the B12-dependent rSAM family (21). Finally, during the course of the work described here, the Layer group reported *in vitro* activity of MgmA from *Methanoculleus thermophilus*, a B12-dependent rSAM methyltransferase responsible for the 2-methylglutamine PTM (22). *In vivo* characterization of *mgmA* mutants has yet to be reported.

Here, we show that MgmA homologs can methylate the target glutamine in McrA *in vivo* when heterologously expressed in *M. acetivorans*, which does not normally contain this PTM. Recombinant strains that express MgmA show small, but significant, growth defects on methylotrophic substrates showing that the methylglutamine PTM effects

MCR activity, a finding that is supported by the observation of altered cofactor binding in the crystal structure of Gln-modified MCR. Structural studies of MgmA reveal a canonical domain B12-dependent rSAM methyltransferase with a large active site suitable for binding unfolded MCR.

RESULTS

Bioinformatic identification of genes involved in PTM of MCR

To identify genes that could be involved in post-translational glutamine methylation, we compared the genomes of *M. marburgensis*, *Methanopyrus kandleri*, and *Methanoterris formicicus*, which have this PTM, to those of *M. acetivorans* and *Methanosarcina barkeri*, which do not. This produced a list of 77 candidates that are present only in strains with this PTM (Table S1). Among these, only two encode rSAM methyltransferases. The first is the *hcgA* family, which is involved in biosynthesis of novel hydrogenase cofactor (23). The second, which we designated *mgmA*, encodes a family of putative B12-dependent rSAM methyltransferases. MgmA homologs are encoded by organisms within every euryarchaeal order that includes methanogens except the *Methanomassiliicoccales* (Fig. 1). Several recently discovered organisms from the TACK superphylum also encode MgmA, as well as MCR and/or the related family of alkyl-CoM reductases (2). Consistent with the idea that *mgmA* plays a role in MCR maturation, we observed the gene to be clustered with the MCR operon in most members of the genera *Methanobacteriales* and *Methanosaeta*. Thus, as previously suggested, MgmA is a strong candidate for synthesis of the methylglutamine residue in MCR (22, 24).

Expression of MgmA in *M. acetivorans* results in glutamine methylation

To show that MgmA is responsible for the 2-methylglutamine PTM, we expressed the gene from two different methanogens in *M. acetivorans* (14). The gene from the *Methanosaeta harundinacea* was chosen in the hope that the close phylogeny of the two organisms would minimize potential heterologous expression issues; however, because this PTM has not been confirmed in *M. harundinacea*, we also expressed the *mgmA* from *M. marburgensis*, where it is known to occur (5, 25). Each gene was placed under the control of a tightly regulated promoter and inserted into the *M. acetivorans* chromosome in single copy. After growth of these strains with and without inducer, MCR was analyzed via electrospray ionization mass spectrometry (ESI-MS/MS) to establish the MCR methylation state of the peptide containing the Gln₄₂₀ target residue (Fig. 2; Fig. S1 and S2). When the *M. harundinacea* protein (*MhMgmA*) was expressed, approximately 2% of the target peptide had a mass 14 Da heavier, consistent with a single methylation event. MS/MS analysis of the heavier peptide localized the modification to a 4-amino acid region containing Gln₄₂₀. Thus, *MhMgmA* can methylate *M. acetivorans* McrA *in vivo*, albeit poorly. To test whether the poor activity of *MhMgmA* was due to differences in the target sequence between *M. harundinacea* and *M. acetivorans*, we used Cas9-dependent genome editing to change the McrA target sequence of *M. acetivorans* so that the eight upstream, and nine downstream, amino acids were identical to those in *M. harundinacea* McrA. This led to fivefold increase in the amount of the heavier peptide, showing that the altered target sequence improves enzyme activity, but not enough to achieve full methylation of McrA. In contrast, the strain expressing the *M. marburgensis* protein (*MmMgmA*) showed nearly complete (*ca.* 95%) modification of the target peptide (Fig. 2; Fig. S3). Thus, *MmMgmA* is an efficient methylase of *M. acetivorans* McrA, despite several differences between the target peptides of the native organisms. Methylation was not observed when the strains were grown under non-inducing conditions.

Phenotypic consequences of Gln₄₂₀ methylation in *M. acetivorans*

We measured the doubling time and cell yield of *M. acetivorans* expressing *Mm-mgmA* in methanol and trimethylamine (TMA) media to assess the effect of the modified MCR on growth. To ensure that the phenotypes were due to Gln methylation, rather than the

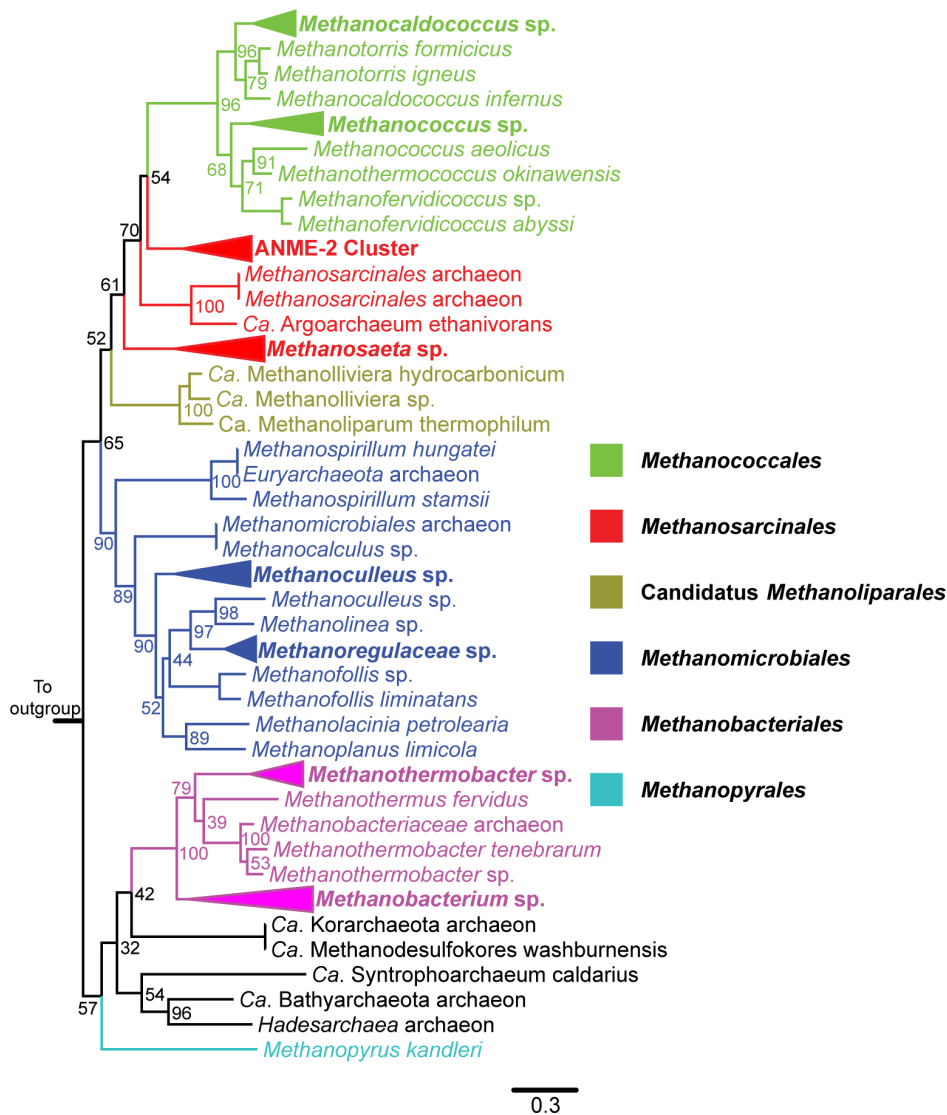


FIG 1 The phylogeny of MgmA homologs. A maximum-likelihood phylogenetic tree of MgmA homologs is shown. Branches are color-coded based on the archaeal order of the organisms in which each homolog is found, as indicated by the key within the figure. The node labels indicate bootstrap support of 100 resamples. MiaB, an rSAM protein responsible for tRNA modification in bacteria, was used as an outgroup used to root the tree.

metabolic burden of expressing a foreign protein, we also constructed isogenic strains that express an inactive *mgmA* allele in which the three iron-binding cysteine residues of the essential 4Fe/4S cluster were mutated to alanine. Small, but statistically significant, phenotypic differences were observed between strains expressing the active and inactive alleles of *MmMgmA* (Table 1). Thus, strains expressing the functional allele grew slightly faster on TMA at all temperatures, but with slightly lower growth yields, whereas they grew slightly slower on methanol, without any impact on yield.

Biochemical and structural characterization of MgmA

MhMgmA and *MmMgmA* were anoxically purified and biochemically characterized after heterologous expression in *M. acetivorans*. The UV-vis spectrum of the as-isolated proteins show a peak at 375 nm with a broad shoulder extending to *ca.* 450 nm, suggesting the presence of intact 4Fe-4S clusters and a cobamide cofactor (Fig. 3). The cofactor was extracted from purified *MmMgmA* and subjected to matrix-assisted laser

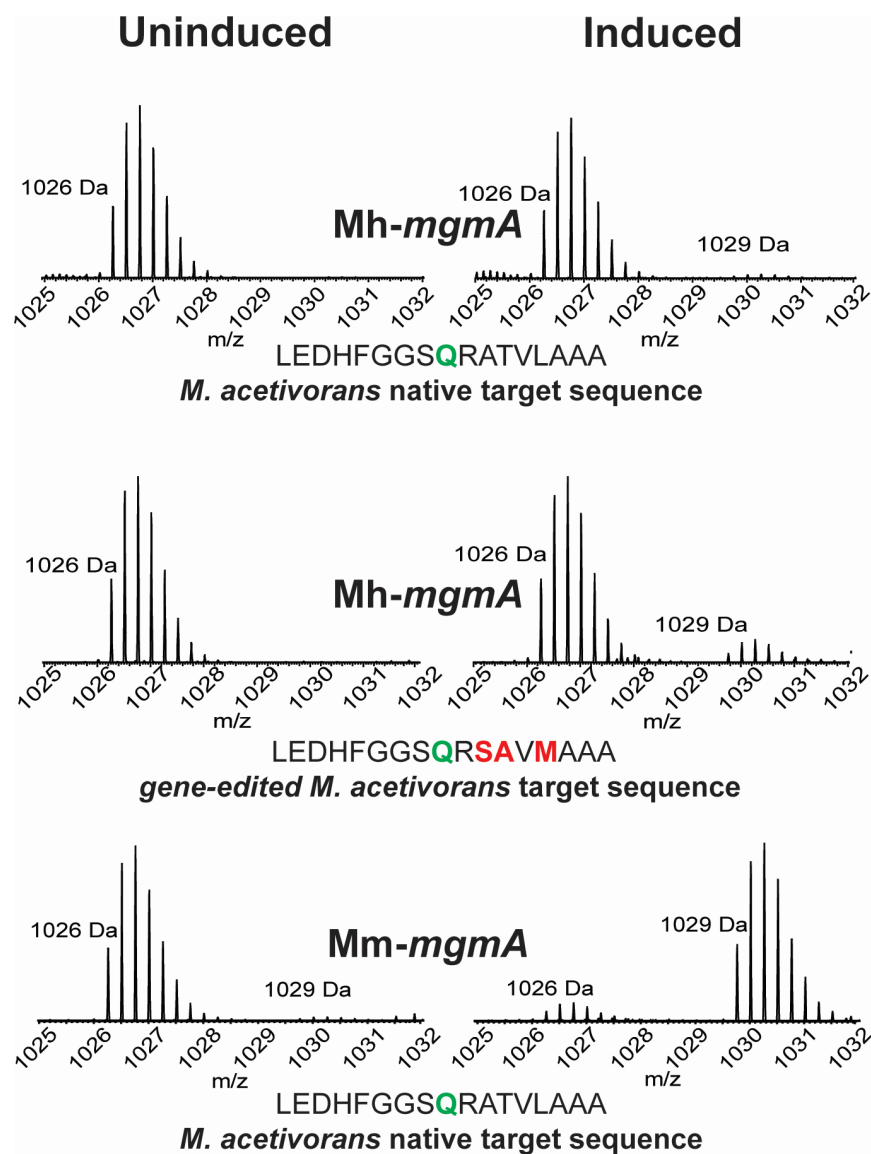


FIG 2 MgmA methylates Gln₄₂₀ of McrA when expressed in *M. acetivorans*. MCR was purified from recombinant *M. acetivorans* strains carrying tightly regulated copies of either *Mh-mgmA* or *Mm-mgmA* after growth under inducing and non-inducing conditions and then subjected to trypsin digestion and mass spectrometric analysis. The ESI-MS spectra of the McrA peptide containing the target glutamine are shown, with uninduced and induced samples on the left and right of each panel, as indicated. The top panel shows the spectrum from an *M. acetivorans* strain expressing *Mh-mgmA*; the middle panel, the spectrum from an *Mh-mgmA*-expressing strain in which McrA has gene-edited to match the local sequence of *M. harundinacea* expressing *Mh-mgmA*; the bottom panel shows the spectrum from an *Mm-mgmA*-expressing strain. The target sequence is shown for each panel, with the target residue in green and mutated residues in red. The series of peaks beginning at m/z of 1,026.2622 ($z = 4$) are consistent with an unmethylated peptide, while those beginning at m/z of 1,029.7663 ($z = 4$) are consistent with a single methylation. MS/MS analysis of the methylated peptides confirms the identity of the indicated peaks, as well as localizing the mass shift to a 2–4 amino acid region containing Gln₄₂₀ (Fig. S1 to S3).

desorption ionization-time of flight-MS (MALDI-TOF-MS), which revealed an intact mass consistent with a cobamide containing 5-hydroxybenzimidazole as the lower ligand, which is the native cobamide found in methanogens (22, 26). The *in vitro* methylation

TABLE 1 Growth phenotypes of *M. acetivorans* expressing active Mm-MgmA (MgmA^{act}) and the inactive Mm-MgmA (MgmA^{inact}) on different substrates and temperatures^a

Conditions ^b	MgmA ^{act} doubling time (hr)	MgmA ^{inact} doubling time (hr)	MgmA ^{act} max OD ₆₀₀	MgmA ^{inact} max OD ₆₀₀
TMA 30°C	19.2 ± 0.7	21.7 ± 1.1	3.3 ± 0.3	4.1 ± 0.5
TMA 36°C	10.6 ± 0.2	12.7 ± 0.3	3.2 ± 0.2	4.1 ± 0.2
TMA 42°C	11.1 ± 0.9	13.9 ± 1.3	3.4 ± 0.4	4.1 ± 0.2
MeOH 30°C	20.5 ± 1.5	17.9 ± 0.5	4.3 ± 0.5	4.6 ± 0.2
MeOH 36°C	11.8 ± 0.3	9.5 ± 0.7	4.0 ± 0.3	4.0 ± 0.3
MeOH 42°C	14.9 ± 1.0	12.6 ± 1.3	3.4 ± 0.2	3.6 ± 0.2

^aValues represent the mean and 95% confidence intervals for three biological replicates. Differences with a $P < 0.05$ (calculated using a two-tailed t -test assuming equal variances) were considered significant and are highlighted in bold.

^bTMA, trimethylamine; MeOH, methanol.

activity of the as-purified proteins was assessed via mass spectrometric analysis of a 20-amino acid peptide substrate corresponding to the target region of the *M. acetivorans* McrA. Although *MmMgmA* was significantly more active, both enzymes were able to methylate the peptide substrate, with 76% and 39% of the substrate being consumed in overnight reactions of *MmMgmA* and *MhMgmA*, respectively.

To obtain larger amounts of the enzyme, *MmMgmA* was expressed in *Escherichia coli*, followed by *in vitro* reconstitution using a commercially available cobamide containing dimethylbenzimidazole as the lower ligand (Fig. S4). Efficient reconstitution was validated by quantification of iron (3.3 ± 0.4 per protein) and cobalamin (0.89 per protein). The reconstituted enzyme was highly active, with k_{cat} values of 0.31 and 0.19 min⁻¹ determined by quantification of the reaction products 5'-dAH and SAH, respectively. Subsequent anoxic crystallization allowed determination of a 2.08 Å structure that is similar to other B12-dependent rSAM methyltransferases (Fig. S5, [27, 28]), with a large active site cleft (Fig. 4). Like other B12-dependent rSAM methyltransferases, the benzimidazole tail anchors the Cbl cofactor (dimethylbenzimidazole in the reconstituted enzyme) in the active site tucked into the Rossmann fold domain and does not serve as the lower ligand of the cofactor (Fig. S6, [27]). Previously characterized B12-dependent rSAMs have a hydrophobic amino acid in the lower axial position of the Cbl cofactor, which is absent in *MmMgmA* (28). The closest residue that could serve this function is Gln₄₉, which is 8.3 Å away and facing the wrong direction. The lack of a lower cobalt ligand is consistent with electron paramagnetic resonance (EPR) data reported by Gagsteiger et al. (22); however, when rotated around its β-carbon, the amine of Gln₄₉ is ideally placed for coordination to the cofactor with a distance of 2.5 Å (Fig. S6), suggesting a possible alternative that may have implications during catalysis.

Structure and redox state of Gln₄₂₀-methylated MCR from *M. acetivorans* (*MaMCR*)

To assess whether Gln₄₂₀ methylation alters the structure of MCR, we aerobically purified the Ni(II) form of affinity-tagged *MaMCR* from a strain expressing *MmMgmA*, allowing determination of structure at 2.0 Å resolution (Fig. 5; Fig. S7). The protein fold seen in the structure is nearly identical to that of the unmodified enzyme with a mean RMSD of 0.25 Å. Clear electron density is seen for α-methylation on Gln₄₂₀, consistent with the studies described above. Surprisingly, the active site contains the CoM-S-S-CoB heterodisulfide positioned near the Ni(II)-F₄₃₀, whereas free CoM and CoB was observed in each of the eight prior *MaMCR* structures we have obtained (14, 16). The Ni(II) is coordinated by four nitrogen atoms of the tetrapyrrole of F₄₃₀, the side chain oxygen of Gln₁₆₁, and the sulfonate oxygen of the heterodisulfide. Although dozens of MCR structures have been reported (including eight from *M. acetivorans*), the bound heterodisulfide has only been observed once before, in the MCR silent form of the

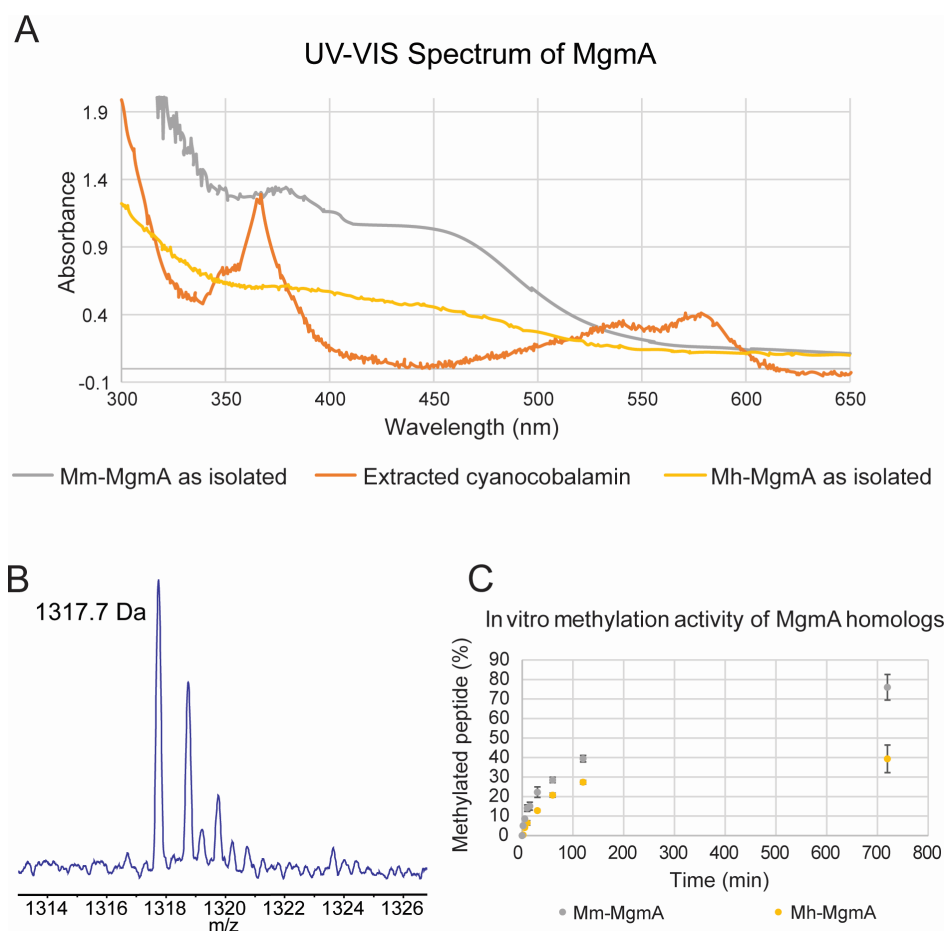


FIG 3 Biochemical characterization of affinity-purified MgmA. (A) UV-vis spectra of as-isolated Mh-MmgA (yellow trace) Mm-MgmA (grey trace), and cyanocobalamin extracted from the Mm-MgmA (orange trace). UV-vis spectra of Mh-MgmA as isolated (yellow). (B) Ion intensity chromatogram of the major peak observed by MALDI-TOF-MS of the cyano-cobalamine derivative of the cofactor extracted from Mm-MmgA. The cobamide was confirmed to have 5-hydroxybenzimidazolyl as the lower ligand based on the observed mass of 1,317.738 (m/z) relative to the predicted exact mass of 1,317.535 (m/z). (C) Methylation activity of Mm-MgmA (yellow trace) and Mm-MgmA (grey trace) using a peptide substrate. The amounts of methylated peptide were determined by MALDI-TOF-MS at the indicated timepoints, with the average and standard deviation of triplicate assays shown.

enzyme isolated from of *M. marburgensis* (formerly *Methanobacterium thermoautotrophicum*, PDB Code 1HBM [25]).

To examine whether Gln₄₂₀ methylation affected the redox state of the F₄₃₀ cofactor, modified and unmodified MaMCRs were also isolated under strictly anoxic, highly reducing conditions. The UV-vis spectrum suggests that the majority of the enzyme in both the modified and unmodified preparations is in the MCR-silent Ni(II) state displaying maximum absorbance at 420 nm, with a shoulder at 445 nm (Fig. S8A). Analysis by EPR shows that MCRox1 forms are present in both modified and unmodified MaMCR, with ca. twofold more in the Gln-methylated derivative (Fig. S8B). However, due to data processing issues associated with the strong the Ti-citrate buffer signal, these values have an appreciable systematic error. Thus, we are hesitant to draw strong conclusions from these data.

DISCUSSION

The data presented here show that MgmA family members methylate the Gln₄₂₀ residue in McrA *in vivo* and are fully consistent with *in vitro* results obtained with the homolog

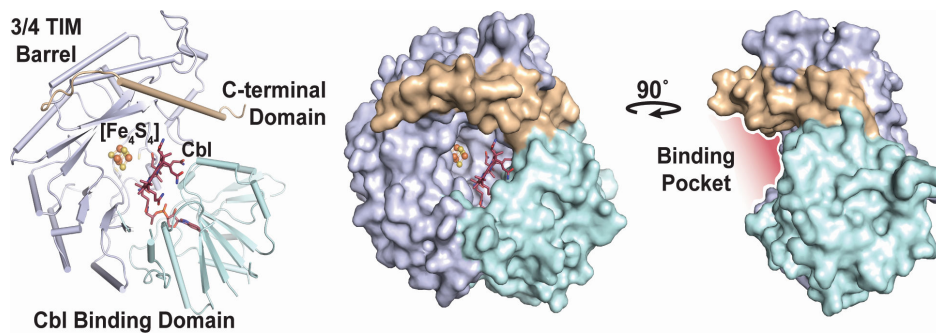


FIG 4 X-ray crystal structure of *MmMgmA* with bound cofactors. The architecture of *MmMgmA* showing the Rossman fold (pale cyan) with bound cobalamin (red), $\frac{3}{4}$ TIM barrel (light blue) with the rSAM [Fe₄S₄] cluster coordinated by three cysteines, and the C-terminal domain (wheat) is shown on the left. A surface view of *MmMgmA* revealing the active site opening from the front is shown in the center, with a large peptide binding cleft (red) revealed when the protein is rotated 90 degrees clockwise on the right.

from *M. thermophilus* (22). Interestingly, the MgmA homologs characterized here vary in their methylation activity both *in vivo* and *in vitro*, which is only partially due to differences in the native McrA substrates. This suggests that the enzyme has a limited amount of time to methylate G₄₂₀ before it becomes inaccessible due to protein folding, an idea that is consistent with the large active site cleft of *MmMgmA* that presumably binds a linear, unfolded peptide substrate.

The key question that has yet to be answered is why some methanogens methylate Gln₄₂₀, while others do not. Based on available MCR structures, the methyl moiety fills a gap that is occupied by water in MCRs without this PTM (11). In *M. barkeri* MCR, this water molecule is part of a hydrogen-bonding network that positions Tyr₃₄₆ for hydrogen bonding with the axial Ni-ligand in F₄₃₀, which is presumably required for efficient catalysis. This key water is held in place via a hydrogen-bond with the nearby Thr₄₂₃ residue, a position that is occupied by Ala in MCRs that have Gln methylation (5). It has been suggested that by filling the gap occupied by this key water molecule, the methyl-Gln PTM also serves to position Tyr₃₄₆ for hydrogen bonding with the axial Ni-ligand (11). Identification of MgmA as the Gln methylase allows us to extend this analysis to a much larger collection of strains. Accordingly, we examined 154 methanogen genomes, which encode 204 McrA homologs due to the fact that some species have two MCR isozymes (Data Set S1). Of these, 62 encode MgmA. Strikingly, 84 of the 85 MCRs found in organisms that encode MgmA have a small hydrophobic residue (always Gly or Ala) in the position analogous to Thr₄₂₃, the only exception being one of the two MCRs encoded by *Methanobacterium formicicum* Mb9. However, when the McrA position analogous to Thr₄₃₂ is occupied by a hydrogen bond donor (always Ser or Thr), the organisms almost never encode MgmA (again the only exception is *M. formicicum* Mb9). These data lend credence to the idea that alternate mechanisms for positioning of Tyr₃₄₆ are important. Nevertheless, it is important to note that the hydrogen-bonding network, including the water molecule in question, remains intact in our Gln-modified *MaMCR* structure. Thus, the additional methyl group is insufficient to displace water when Thr₄₂₃ is present. It should also be noted that *ca.* one-third of the organisms with Ala or Gly in this position lack MgmA. Therefore, it remains possible that these alternate conformations have distinct functions in organisms with and without methylglutamine. In this regard, it is interesting to note that most of the organisms lacking MgmA are capable of methylotrophic methanogenesis (Data Set S2). Because the vast majority of these methylotrophic methanogens fall within the *Methanosarcinales*, this could be a reflection of phylogeny rather than function, but significant phylogenetic outliers suggest this is not the case. For example, both *Methanobrevibacter* and *Methanospheara* species lack MgmA and are capable of using methanol (29), whereas other genera within the *Methanobacteriales* encode MgmA and are incapable of using methanol. Similarly,

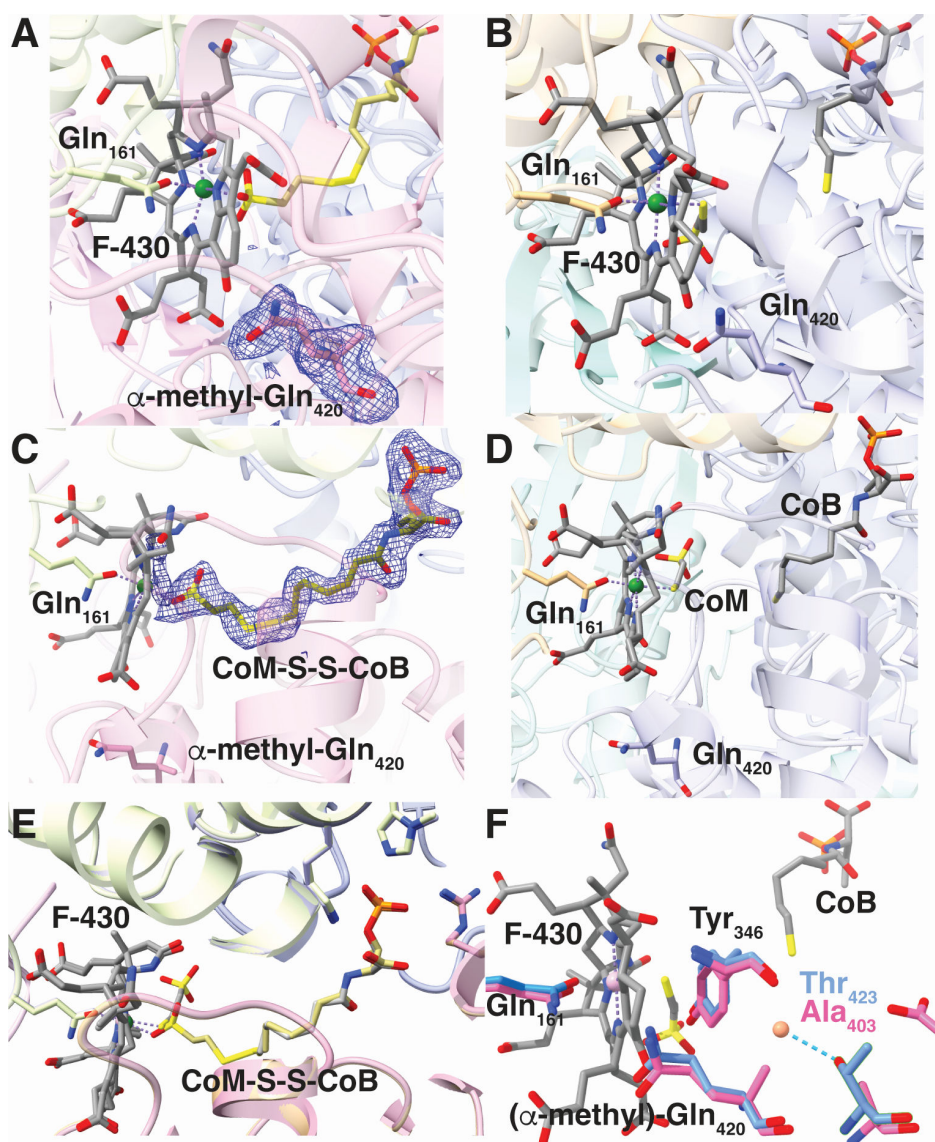


FIG 5 Active site of MaMCR with and without Gln₄₂₀ methylation. (A) The active site of MaMCR purified from a strain expressing *MmMgmA*, with the outlined electron density clearly showing methylation of Gln₄₂₀. (B) The same view as in panel A for unmodified MaMCR. (C) A side view of Gln₄₂₀-methylated MaMCR showing the bound CoM-S-S-CoB heterodisulfide coordinated to the F430 cofactor via the sulfonate moiety of CoM. The position α -methyl-Gln₄₂₀ is also shown. (D) The same view as in panel C for unmodified MaMCR showing the positions of the free CoM and CoB cofactors, as well as the unmodified Gln₄₂₀. (E) Superposition of the structures of unmodified and modified MaMCR in the vicinity of the CoM and CoB cofactors showing strong conservation of active site features. (F) Superposition of the active sites of unmodified MaMCR and *MmMCR* (which contains a MeGln residue) showing adaptations that accommodate the methyl group. The water molecule H-bonded to Thr₄₂₃ is shown as an orange sphere.

members of the methylotrophic orders *Methanomassiliococcales*, *Methanomethylales*, and *Methanonatronarchaeales* also lack MgmA. Although the correlation between MgmA absence and methylotrophy is not absolute, these findings suggest that there may be a functional linkage. As we have previously noted (14), methylated substrates are assimilated directly into methyl-CoM, and it is therefore that the cytoplasmic concentration of this substrate differs between methylotrophic, hydrogenotrophic, and acetlastic methanogens that form methyl-CoM in a different fashion. It is tempting to speculate

that the hydrogen-bonding network of methanogens without methylglutamine serves to tune the substrate affinity of the enzyme to higher methyl-CoM concentrations.

Regardless of the function(s) of methyl-Gln and the analogous hydrogen-bonding network, perturbation of this critical region in the active site affects MCR function. This can be seen in two ways. First, phenotypic characterization of *M. acetivorans* strains with and without the 2-methylglutamine PTM revealed statistically significant differences in the use of methylotrophic substrates. While this effect is small, it is important to note that MCR is not the rate-limiting step in the growth of *M. acetivorans*. Indeed, a recent study by the Nayak group showed that MCR expression can be lowered by ~70% before a growth phenotype can be observed (30). Thus, the observation of any phenotype suggests that the enzyme activity has been significantly reduced. Indeed, we cannot exclude the possibility that all growth depends on the small fraction (*ca.* 5%) of unmethylated MCR (see Fig. 2). Second, the Gln modification in *MaMCR*, which also contains the Thr₄₂₃-dependent hydrogen bonding network, alters the binding of the CoM-S-S-CoB heterodisulfide in way that allows this reaction product to remain bound during enzyme purification, as opposed to the free cofactors seen in each of the eight previous *MaMCR* structures that we have obtained (14, 16). This suggests that product release has been altered by the modification. Experiments to identify the nature of this perturbation (e.g., effects on K_m , k_{cat}) will await the development of methods to purify the active Ni(I) state of *M. acetivorans* MCR, or the development of efficient genetics for organisms like *M. marburgensis*, from which active MCR can be purified. Unfortunately, neither approach is currently feasible, although recent progress in the development of genetic tools for *M. marburgensis* holds promise for solving this issue (31).

MATERIALS AND METHODS

Bioinformatics methods

Standard bioinformatics analyses were performed using webtools available on the National Center for Biotechnology Information website. Phylogentic profiling was performed using tools available on the Department of Energy's Integrated Microbial Genomes website. The protein classification and neighborhood networks were generated using tools of the Enzyme Function Initiative (32).

Molecular biology methods

Standard molecular biology methods were used throughout. Details of most plasmid constructions are provided in Table S2. Primers and synthetic DNA fragments used in these constructions are listed in Tables S3 and S4. CRISPR gene editing target sequences are listed in Table S5. Plasmid *pMmMgmA* was used for expression of *MmMgmA* in *E. coli* and was made by cloning a codon-optimized derivative into pET28a. All plasmids were verified by Sanger sequencing at the Roy J. Carver Biotechnology Center, University of Illinois Urbana-Champaign or the Pennsylvania State Genomics Core Facility.

Construction and growth of microbial strains

Methods for growth and genetic manipulation of *E. coli* and *M. acetivorans* have been previously described (33–35). *M. acetivorans* strains generated in this project were verified by Sanger sequencing of PCR products containing the modified regions at the Roy J. Carver Biotechnology Center, University of Illinois Urbana-Champaign.

Purification and mass-spectrometric analysis of *M. acetivorans* MCR

MCR for mass spectrometric analyses of protein modification was purified under aerobic conditions using ammonium sulfate precipitation followed by size exclusion chromatography essentially as described (36). The modification state of MCR was determined by high-resolution electrospray ionization (ESI) MS/MS a Thermo Fisher Scientific Orbitrap Fusion ESI-MS as previously described (14, 16).

Growth assays for *M. acetivorans* strains

M. acetivorans strains were grown in single cell morphology in high-salt medium (37, 38) containing either 125-mM methanol or 50-mM TMA. Growth rate was quantified by measuring the OD at a wavelength of 600 nm using a Spectronic 200E (Thermo Fisher Scientific) spectrophotometer.

Purification and characterization of MgmA from *M. acetivorans*

TAP-tagged MgmA was purified under anoxic conditions as described (16) with the following changes: lysis buffer was 50-mM HEPES, pH 7.5, 10-mM DTT, wash buffer was 250-mM KCl, and elution buffer was 250-mM KCl with 50-mM biotin. The cobamide cofactor was extracted and identified by mass-spectrometric analysis as previously described (39). MgmA activity assays were performed in triplicate under strictly anoxic conditions at 25°C. The reaction mixture was composed of 20-mM HEPES (pH7.5), 150- μ M peptide substrate and 2-mM Ti(III) citrate, 7.5- μ M MgmA. The reaction was initiated by addition of SAM to a final concentration of 500- μ M. The reaction was quenched by adding an equal volume of 100-mM H₂SO₄ and then analyzed via MALDI-TOF-MS using alpha-cyano-4-hydroxycinnamic acid (CHCA) and matrix and a Bruker UltrafleXtreme Mass Spectrometer (Bruker Daltonics, Billerica, MA, USA) in a reflector-positive mode at the University of Illinois School of Chemical Sciences Mass Spectrometry Laboratory. Peptide concentrations were calculated by measuring the ratio between the modified and unmodified peptides (40).

Purification and characterization of MgmA from *E. coli*

Expression, purification, and reconstitution of *Mm*MgmA were modified from previously established methods after heterologous expression in *E. coli* BL-21(DE3)/pDB1282/pBAD42-BtuCEDF/p*Mm*MgmA (41, 42). Purified protein was designated “as isolated *Mm*MgmA (AI *Mm*MgmA)” prior to reconstitution and “reconstituted *Mm*MgmA (RCN *Mm*MgmA)” following the restoration of the 4Fe-4S cluster and insertion of the cobamide. Fe content of the reconstituted protein was determined as previously described (43). Activity assays contained 20- μ M RCN *Mm*MgmA, 200- μ M peptide substrate, 500- μ M SAM, 2-mM TiCitrate, 250-mM KCl, and 100- μ M D-methionine-methyl-d₃ in 50-mM HEPES, pH 7.5. Assays were quenched by a twofold dilution in 100-mM sulfuric acid at each time point. 5'dAH, methionine, and S-adenosylhomocysteine were quantified after separation on an Agilent Technologies 1290 Infinity II series UHPLC system coupled to a 6470 QQQ Agilent Jet Stream electrospray-ionization mass spectrometer equipped with Agilent Zorbax Extend-C18 RRHD column (2.1 mm \times 50 mm, 1.8- μ m particle size). A standard curve of 5'dAH, Met, and SAH (500 nM through 300 μ M) with 50- μ M D-methionine-methyl-d₃ (internal standard) was prepared for quantification using the Agilent MassHunter Quantitative Analysis 10.1 Software.

Purification of MCR from *M. acetivorans* for crystallography

TAP-tagged MCR was purified under aerobic conditions as described (14) except that crystallography buffer composed of 100-mM Tris-HCl and 300-mM NaCl (pH 8) was used for washing steps after protein binding. Proteins were eluted using crystallography buffer containing 50mM biotin.

Crystallization of *Ma*MCR Gln₄₂₀ variant

The purified enzyme was concentrated to 25-mg/mL prior to crystallization via ultrafiltration. The crystallization trials utilized 2- μ L sitting drops composed of 0.9:0.9:0.2 (protein:reservoir solution:additive screen) that were equilibrated against a 500- μ L volume of the reservoir solution at room temperature. The reservoir solution contained 0.2-M ammonium acetate, 0.1-M sodium acetate (pH = 4), and 15%–20% (wt/vol) PEG 4000. Prior to freezing by vitrification in liquid nitrogen, crystals were soaked in reservoir

solution supplemented with an additional 20% (vol/vol) glycerol or 30% (wt/vol) PEG 4000. Diffraction data were collected at MacCHESS using a Dectris Eiger2 detector. Raw diffraction images were integrated and scaled using either XDS or AutoProc. Molecular replacement was carried out using the coordinates for the structure of wild-type *MaMCR*. The initial model was subject to manual rebuilding, and cofactors were added to the model after the free R factor dropped below 0.30. Relevant crystallographic statistics are detailed in Table S7.

***MmMgmA* structure determination by X-ray crystallography**

RCN *MmMgmA* crystals were generated via the hanging drop vapor diffusion method at room temperature by mixing 1 μ L of a solution of *MmMgmA* in storage buffer (5 mg/mL) with 1 μ L of the well solution (0.2-M calcium chloride, 20% [wt/vol] PEG 3350, and 5-mM SAH). Crystals were prepared for data collection by mounting on rayon loops followed by soaking in cryoprotectant solution (50% [wt/vol] PEG 3350) and flash-freezing in LN. The structures were determined by single anomalous dispersion phasing using Autosol/HySS or by molecular replacement using the program PHASER (44). Model building and refinement were performed with Coot and phenix.refine, respectively (45, 46). Ligand geometric restraints were obtained from the Grade Web Server (<https://www.globalphasing.com>). Structures were validated and analyzed for Ramachandran outliers with the Molprobtity server (47). Figures were prepared using PyMOL. Active site cavity mapping was prepared using Hollow (48). Data collection and refinement statistics are provided in Table S8.

ACKNOWLEDGMENTS

We acknowledge the Division of Chemical Sciences, Geosciences, and Biosciences, Office of Basic Energy Sciences of the US Department of Energy through Grant DE-FG02-02ER15296 for funding to W.M. This work was also supported by the NIH (GM122595 to S.J.B.) and the Eberly Family Distinguished Chair in Science (S.J.B.). S.J.B. is an investigator of the Howard Hughes Medical Institute.

This research used resources of the Advanced Photon Source, a US Department of Energy (DOE) Office of Science User Facility operated for the DOE Office of Science by Argonne National Laboratory under Contract No. DE-AC02-06CH11357. Use of GM/CA@APS has been funded in whole or in part with Federal funds from the National Cancer Institute (ACB-12002) and the National Institute of General Medical Sciences (AGM-12006). The Eiger 16M detector at GM/CA-XSD was funded by National Institutes of Health (NIH) grant S10 OD012289. Use of the LS-CAT Sector 21 was supported by the Michigan Economic Development Corporation and the Michigan Technology Tri-Corridor (Grant 085P1000817). This research also used the resources of the Berkeley Center for Structural Biology supported in part by the Howard Hughes Medical Institute. The Advanced Light Source is a Department of Energy Office of Science User Facility under Contract No. DE-AC02-05CH11231. The ALS-ENABLE beamlines are supported in part by the NIH, National Institute of General Medical Sciences, grant P30 GM124169.

AUTHOR AFFILIATIONS

¹Department of Microbiology, University of Illinois Urbana-Champaign, Champaign, Illinois, USA

²Department of Chemistry, Pennsylvania State University, University Park, Pennsylvania, USA

³Department of Biochemistry, University of Illinois Urbana-Champaign, Champaign, Illinois, USA

⁴Department of Chemistry, University of Illinois Urbana-Champaign, Champaign, Illinois, USA

⁵Center for Biophysics and Quantitative Biology, University of Illinois Urbana-Champaign, Champaign, Illinois, USA

⁶Department of Biochemistry and Molecular Biology, Pennsylvania State University, University Park, Pennsylvania, USA

⁷The Howard Hughes Medical Institute, Pennsylvania State University, University Park, Pennsylvania, USA

AUTHOR ORCID*s*

Roy J. Rodriguez Carrero  <http://orcid.org/0000-0001-8447-5641>

William Metcalf  <http://orcid.org/0000-0002-0182-0671>

FUNDING

Funder	Grant(s)	Author(s)
U.S. Department of Energy (DOE)	DE-FG02-02ER15296	William Metcalf
HHS National Institutes of Health (NIH)	GM122595	Squire J. Booker
U.S. Department of Energy (DOE)	DE-AC02-06CH11357	Squire J. Booker
HHS National Institutes of Health (NIH)	S10 OD012289	Squire J. Booker
U.S. Department of Energy (DOE)	DE-AC02-05CH11231	Squire J. Booker
HHS National Institutes of Health (NIH)	P30 GM124169	Squire J. Booker
HHS NIH National Cancer Institute (NCI)	ACB-12002	Squire J. Booker
HHS National Institutes of Health (NIH)	AGM-12006	Squire J. Booker
Michigan Economic Development Corporation and the Michigan Technology Tri-Corridor	085P1000817	Squire J. Booker

AUTHOR CONTRIBUTIONS

Roy J. Rodriguez Carrero, Conceptualization, Formal analysis, Investigation, Methodology, Visualization, Writing – original draft, Writing – review and editing | Cody T. Lloyd, Conceptualization, Data curation, Formal analysis, Investigation, Methodology, Visualization, Writing – original draft, Writing – review and editing | Janhavi Borkar, Formal analysis, Investigation, Writing – original draft, Writing – review and editing | Shounak Nath, Formal analysis, Investigation, Visualization, Writing – original draft, Writing – review and editing | Liviu M. Mirica, Formal analysis, Supervision, Visualization, Writing – original draft, Writing – review and editing | Satish Nair, Formal analysis, Supervision, Visualization, Writing – original draft, Writing – review and editing | Squire J. Booker, Formal analysis, Funding acquisition, Supervision, Writing – original draft, Writing – review and editing | William Metcalf, Conceptualization, Data curation, Formal analysis, Funding acquisition, Investigation, Methodology, Project administration, Resources, Supervision, Validation, Visualization, Writing – original draft, Writing – review and editing

DIRECT CONTRIBUTION

This article is a direct contribution from William Metcalf, a Fellow of the American Academy of Microbiology, who arranged for and secured reviews by Stephen W. Ragsdale, University of Michigan Medical School, and John W. Peters, The University of Oklahoma.

DATA AVAILABILITY

The structural data for *M. acetivorans* MCR containing the 2-methylglutamine modification and for *M. marburgensis* MgmA have been deposited in Protein Data Bank (PDB) under the accession numbers [9ECN](#) and [9CCB](#), respectively.

ADDITIONAL FILES

The following material is available [online](#).

Supplemental Material

Data set S1 (mBio03546-24-s0001.xlsx). Amino acids found at McrA position 432 and cooccurrence of MgmA.

Data set S2 (mBio03546-24-s0002.xlsx). Presence of methylotropic genes and cooccurrence of MgmA.

Supplemental Material (mBio03546-24-s0003.pdf). Supplemental text, tables, and figures.

REFERENCES

- Zinder SH. 1993. Physiology and ecology of methanogens, p 128–206. In Ferry JG (ed), *Methanogenesis: ecology, physiology, biochemistry and genetics*. Chapman and Hall, New York.
- Thauer RK. 2019. Methyl (alkyl)-coenzyme M reductases: nickel F-430-containing enzymes involved in anaerobic methane formation and in anaerobic oxidation of methane or of short chain alkanes. *Biochemistry* 58:5198–5220. <https://doi.org/10.1021/acs.biochem.9b00164>
- Wongnate T, Sliwa D, Ginovska B, Smith D, Wolf MW, Lehnert N, Raugei S, Ragsdale SW. 2016. The radical mechanism of biological methane synthesis by methyl-coenzyme M reductase. *Science* 352:953–958. <https://doi.org/10.1126/science.aaf0616>
- Jaun B, Thauer RK. 2007. Methyl-coenzyme M reductase and its nickel corphin coenzyme F430 in methanogenic archaea. *Met Ions Life Sci* 2:323–356. <https://doi.org/10.1002/9780470028131>
- Ermiler U, Grabarse W, Shima S, Goubeaud M, Thauer RK. 1997. Crystal structure of methyl-coenzyme M reductase: the key enzyme of biological methane formation. *Science* 278:1457–1462. <https://doi.org/10.1126/science.278.5342.1457>
- Hahn CJ, Lemaire ON, Kahnt J, Engilberge S, Wegener G, Wagner T. 2021. Crystal structure of a key enzyme for anaerobic ethane activation. *Science* 373:118–121. <https://doi.org/10.1126/science.abg1765>
- Kahnt J, Buchenau B, Mahler F, Krüger M, Shima S, Thauer RK. 2007. Post-translational modifications in the active site region of methyl-coenzyme M reductase from methanogenic and methanotrophic archaea. *FEBS J* 274:4913–4921. <https://doi.org/10.1111/j.1742-4658.2007.06016.x>
- Shima S, Krueger M, Weinert T, Demmer U, Kahnt J, Thauer RK, Ermiler U. 2011. Structure of a methyl-coenzyme M reductase from Black Sea mats that oxidize methane anaerobically. *Nature New Biol* 481:98–101. <https://doi.org/10.1038/nature10663>
- Wagner T, Kahnt J, Ermiler U, Shima S. 2016. Didehydroaspartate modification in methyl-coenzyme M reductase catalyzing methane formation. *Angew Chem Int Ed Engl* 55:10630–10633. <https://doi.org/10.1002/anie.201603882>
- Wagner T, Wegner CE, Kahnt J, Ermiler U, Shima S. 2017. Phylogenetic and structural comparisons of the three types of methyl coenzyme M reductase from *Methanococcales* and *Methanobacteriales*. *J Bacteriol* 199:e00197-17. <https://doi.org/10.1128/JB.00197-17>
- Grabarse W, Mahler F, Shima S, Thauer RK, Ermiler U. 2000. Comparison of three methyl-coenzyme M reductases from phylogenetically distant organisms: unusual amino acid modification, conservation and adaptation. *J Mol Biol* 303:329–344. <https://doi.org/10.1006/jmbi.2000.4136>
- Lemaire ON, Wagner T. 2022. A structural view of alkyl-coenzyme M reductases, the first step of alkane anaerobic oxidation catalyzed by Archaea. *Biochemistry* 61:805–821. <https://doi.org/10.1021/acs.biochem.2c00135>
- Kurth JM, Müller MC, Welte CU, Wagner T. 2021. Structural insights into the methane-generating enzyme from a methoxydotrophic methanogen reveal a restrained gallery of post-translational modifications. *Microorganisms* 9:837. <https://doi.org/10.3390/microorganisms9040837>
- Nayak DD, Mahanta N, Mitchell DA, Metcalf WW. 2017. Post-translational thioamidation of methyl-coenzyme M reductase, a key enzyme in methanogenic and methanotrophic Archaea. *Elife* 6:e29218. <https://doi.org/10.7554/eLife.29218>
- Mahanta N, Liu A, Dong S, Nair SK, Mitchell DA. 2018. Enzymatic reconstitution of ribosomal peptide backbone thioamidation. *Proc Natl Acad Sci U S A* 115:3030–3035. <https://doi.org/10.1073/pnas.1722324115>
- Nayak DD, Liu A, Agrawal N, Rodriguez-Carero R, Dong SH, Mitchell DA, Nair SK, Metcalf WW. 2020. Functional interactions between posttranslationally modified amino acids of methyl-coenzyme M reductase in *Methanosarcina acetivorans*. *PLoS Biol* 18:e3000507. <https://doi.org/10.1371/journal.pbio.3000507>
- Broderick JB, Broderick WE, Hoffman BM. 2023. Radical SAM enzymes: nature's choice for radical reactions. *FEBS Lett* 597:92–101. <https://doi.org/10.1002/1873-3468.14519>
- Sinner EK, Marous DR, Townsend CA. 2022. Evolution of methods for the study of cobalamin-dependent radical SAM enzymes. *ACS Bio Med Chem Au* 2:4–10. <https://doi.org/10.1021/acsbiomedchemau.1c00032>
- Lyu Z, Shao N, Chou CW, Shi H, Patel R, Duin EC, Whitman WB. 2020. Posttranslational methylation of arginine in methyl coenzyme M reductase has a profound impact on both methanogenesis and growth of *Methanococcus maripaludis*. *J Bacteriol* 202:e00654-19. <https://doi.org/10.1128/JB.00654-19>
- Radle MI, Miller DV, Laremore TN, Booker SJ. 2019. Methanogenesis marker protein 10 (Mmp10) from *Methanosarcina acetivorans* is a radical S-adenosylmethionine methylase that unexpectedly requires cobalamin. *J Biol Chem* 294:11712–11725. <https://doi.org/10.1074/jbc.RA119.007609>
- Fyfe CD, Bernardo-García N, Fradale L, Grimaldi S, Guillot A, Brewee C, Chavas LMG, Legrand P, Benjdia A, Berteau O. 2022. Crystallographic snapshots of a B₁₂-dependent radical SAM methyltransferase. *Nat New Biol* 602:336–342. <https://doi.org/10.1038/s41586-021-04355-9>
- Gagsteiger J, Jahn S, Heidinger L, Gericke L, Andexer JN, Friedrich T, Loenarz C, Layer G. 2022. A cobalamin-dependent radical SAM enzyme catalyzes the unique ca⁻-methylation of glutamine in methyl-coenzyme M reductase. *Angew Chem Int Ed Engl* 61:e202204198. <https://doi.org/10.1002/anie.202204198>
- Arriaza-Gallardo FJ, Schaupp S, Zheng YC, Abdul-Halim MF, Pan HJ, Kahnt J, Angelidou G, Paczia N, Hu X, Costa K, Shima S. 2022. The function of two radical-SAM enzymes, HcgA and HcgB, in the biosynthesis of the [Fe]-hydrogenase cofactor. *Angew Chem Int Ed Engl* 61:e202213239. <https://doi.org/10.1002/anie.202213239>
- Deobald D, Adrian L, Schöne C, Rother M, Layer G. 2018. Identification of a unique Radical SAM methyltransferase required for the sp³-C-methylation of an arginine residue of methyl-coenzyme M reductase. *Sci Rep* 8:7404. <https://doi.org/10.1038/s41598-018-25716-x>
- Grabarse W, Mahler F, Duin EC, Goubeaud M, Shima S, Thauer RK, Lamzin V, Ermiler U. 2001. On the mechanism of biological methane formation: structural evidence for conformational changes in methyl-coenzyme M reductase upon substrate binding. *J Mol Biol* 309:315–330. <https://doi.org/10.1006/jmbi.2001.4647>
- Gorris LG, van der Drift C. 1994. Cofactor contents of methanogenic bacteria reviewed. *Biofactors* 4:139–145.
- Bridwell-Rabb J, Li B, Drennan CL. 2022. Cobalamin-dependent radical S-adenosylmethionine enzymes: capitalizing on old motifs for new

- functions. *ACS Bio Med Chem Au* 2:173–186. <https://doi.org/10.1021/acsbioimedchemau.1c00051>
28. Knox HL, Sinner EK, Townsend CA, Boal AK, Booker SJ. 2022. Structure of a B₁₂-dependent radical SAM enzyme in carbapenem biosynthesis. *Nature New Biol* 602:343–348. <https://doi.org/10.1038/s41586-021-04392-4>
29. Poehlein A, Schneider D, Soh M, Daniel R, Seedorf H. 2018. Comparative genomic analysis of members of the genera *Methanosphaera* and *Methanobrevibacter* reveals distinct clades with specific potential metabolic functions. *Archaea* 2018:7609847. <https://doi.org/10.1155/2018/7609847>
30. Chadwick GL, Dury GA, Nayak DD. 2024. Physiological and transcriptomic response to methyl-coenzyme M reductase limitation in *Methanosarcina acetivorans*. *Appl Environ Microbiol* 90:e0222023. <https://doi.org/10.1128/aem.02220-23>
31. Fink C, Beblawy S, Enkerlin AM, Mühlring L, Angenent LT, Molitor B. 2021. A shuttle-vector system allows heterologous gene expression in the thermophilic methanogen *Methanothermobacter thermoautotrophicus* ΔH. *MBio* 12:e0276621. <https://doi.org/10.1128/mBio.02766-21>
32. Oberg N, Zallot R, Gerlt JA. 2023. EFI-EST, EFI-GNT, and EFI-CGFP: enzyme function initiative (EFI) web resource for genomic enzymology tools. *J Mol Biol* 435:168018. <https://doi.org/10.1016/j.jmb.2023.168018>
33. Metcalf WW, Zhang JK, Apolinario E, Sowers KR, Wolfe RS. 1997. A genetic system for Archaea of the genus *Methanosarcina*: liposome-mediated transformation and construction of shuttle vectors. *Proc Natl Acad Sci U S A* 94:2626–2631. <https://doi.org/10.1073/pnas.94.6.2626>
34. Metcalf WW, Zhang JK, Wolfe RS. 1998. An anaerobic, intrachamber incubator for growth of *Methanosarcina* spp. on methanol-containing solid media. *Appl Environ Microbiol* 64:768–770. <https://doi.org/10.1128/AEM.64.2.768-770.1998>
35. Guss AM, Rother M, Zhang JK, Kulkarni G, Metcalf WW. 2008. New methods for tightly regulated gene expression and highly efficient chromosomal integration of cloned genes for *Methanosarcina* species. *Archaea* 2:193–203. <https://doi.org/10.1155/2008/534081>
36. Duin EC, Prakash D, Brungess C. 2011. Methyl-coenzyme M reductase from *Methanothermobacter marburgensis*, p 159–187. In Rosenzweig AC, Ragsdale SW (ed), *Meth enzymol: methods in methane metabolism*, pt A. Metcalf WW, Zhang JK, Shi X, Wolfe RS. 1996. Molecular, genetic, and biochemical characterization of the *serC* gene of *Methanosarcina barkeri* Fusaro. *J Bacteriol* 178:5797–5802. <https://doi.org/10.1128/jb.178.19.5797-5802.1996>
38. Sowers KR, Boone JE, Gunsalus RP. 1993. Disaggregation of *Methanosarcina* spp. and growth as single cells at elevated osmolarity. *Appl Environ Microbiol* 59:3832–3839. <https://doi.org/10.1128/aem.59.11.3832-3839.1993>
39. Fu H, Goettge MN, Metcalf WW. 2019. Biochemical characterization of the methylmercaptopropionate: cob(II)alamin methyltransferase from *Methanosarcina acetivorans*. *J Bacteriol* 201:e00130-19. <https://doi.org/10.1128/JB.00130-19>
40. Szájli E, Fehér T, Medzihradsky KF. 2008. Investigating the quantitative nature of MALDI-TOF MS. *Mol Cell Proteomics* 7:2410–2418. <https://doi.org/10.1074/mcp.M800108-MCP200>
41. Lanz ND, Grove TL, Gogonea CB, Lee KH, Krebs C, Booker SJ. 2012. RlmN and AtsB as models for the overproduction and characterization of radical SAM proteins. *Methods Enzymol* 516:125–152. <https://doi.org/10.1016/B978-0-12-394291-3.00030-7>
42. Lanz ND, Blaszczyk AJ, McCarthy EL, Wang B, Wang RX, Jones BS, Booker SJ. 2018. Enhanced solubilization of class B radical S-adenosylmethionine methylases by improved cobalamin uptake in *Escherichia coli*. *Biochemistry* 57:1475–1490. <https://doi.org/10.1021/acs.biochem.7b01205>
43. Beinert H. 1978. Micro methods for the quantitative determination of iron and copper in biological material. *Methods Enzymol* 54:435–445. [https://doi.org/10.1016/s0076-6879\(78\)54027-5](https://doi.org/10.1016/s0076-6879(78)54027-5)
44. Bunkóczi G, Echols N, McCoy AJ, Oeffner RD, Adams PD, Read RJ. 2013. Phaser.MRage: automated molecular replacement. *Acta Cryst D Biol Cryst* 69:2276–2286. <https://doi.org/10.1107/S0907444913022750>
45. Otwinowski Z, Minor W. 1997. Processing of X-ray diffraction data collected in oscillation mode. *Methods Enzymol* 276:307–326. [https://doi.org/10.1016/S0076-6879\(97\)76066-X](https://doi.org/10.1016/S0076-6879(97)76066-X)
46. Adams PD, Afonine PV, Bunkóczi G, Chen VB, Davis IW, Echols N, Headd JJ, Hung LW, Kapral GJ, Grosse-Kunstleve RW, McCoy AJ, Moriarty NW, Oeffner R, Read RJ, Richardson DC, Richardson JS, Terwilliger TC, Zwart PH. 2010. PHENIX: a comprehensive Python-based system for macromolecular structure solution. *Acta Cryst D Biol Cryst* 66:213–221. <https://doi.org/10.1107/S0907444909052925>
47. Williams CJ, Headd JJ, Moriarty NW, Prisant MG, Videau LL, Deis LN, Verma V, Keedy DA, Hintze BJ, Chen VB, Jain S, Lewis SM, Arendall WB III, Snoeyink J, Adams PD, Lovell SC, Richardson JS, Richardson DC. 2018. MolProbity: more and better reference data for improved all-atom structure validation. *Protein Sci* 27:293–315. <https://doi.org/10.1002/pro.3330>
48. Ho BK, Gruswitz F. 2008. HOLLOW: generating accurate representations of channel and interior surfaces in molecular structures. *BMC Struct Biol* 8:49. <https://doi.org/10.1186/1472-6807-8-49>